PHYSICAL REVIEW D **90,** 096009 (2014)

Regge behavior in effective field theory

John F. Donoghue,[*] Basem Kamal El-Menoufi,[†] and Grigory Ovanesyan[‡]

Department of Physics, University of Massachusetts, Amherst, Massachusetts 01003, USA

(Received 19 May 2014; published 21 November 2014)

We derive the Regge behavior for the forward scattering amplitude in scalar field theory using the method of regions. We find that the leading Regge behavior to all orders can be obtained. Regge physics emerges from a kinematic region that involves the overlap of several modes, so that a careful treatment of the overlap regions is important. The most consistent and efficient approach utilizes graphs containing collinear, anticollinear and Glauber modes, or modes of soft collinear effective theory with Glauber gluons ($SCET_G$).

DOI: 10.1103/PhysRevD.90.096009 PACS numbers: 11.55.Jy, 12.38.Bx, 12.40.Nn

I. INTRODUCTION

One indication that our effective field theory for high energy QCD is incomplete is that it presently does not reproduce Regge phenomena. This is dangerous because Regge behavior can convert logarithms in a scattering amplitude into powers of the energy. In this paper we find Regge behavior in a related effective field theory, and explore the modes that are needed to produce it.

The soft collinear effective theory (SCET) [1] is an effective field theory for QCD that is relevant for describing the dynamics of highly energetic quarks and gluons. In order to obtain the Lagrangian of SCET one divides a single field into modes corresponding to distinct kinematic behavior and keeps leading terms consistent with the power counting. Using these modes individually, one can reconstruct the behavior of the Feynman diagrams of the full theory. Much of the insight into which modes to include has been obtained from original work by Collins, Soper, and Sterman on all-order factorization theorem proofs [2] and from the method of regions [3]. In this method one starts with the QCD Lagrangian and writes down an amplitude to a given order in the perturbation theory and expands it in one of the momentum regions that are identified using the pinch technique and power counting. Overviews with further references can be found in the book by Smirnov [4] or the review by Jantzen [5]. Sometimes the individual modes are not fully kinematically distinct—there are overlap regions where more than one mode is active [6]. These must be carefully dealt with. It will turn out that the Regge physics lives in these overlap regions and involves a complicated interplay of regions and overlaps. The most consistent and efficient way to describe it uses SCET including Glauber modes ($SCET_G$), as will be described below.

The simplified model is that of a scalar field with a trilinear interaction, which can be considered a scalar model for QCD.[1]

$$\mathcal{L} = \frac{1}{2}\partial_\mu\phi\partial^\mu\phi - \frac{g}{3!}\phi^3. \tag{1}$$

The kinematic region where Regge behavior emerges is $s \to \infty$, t fixed. In such theory, the leading Regge behavior appears from summing an infinite set of ladder graphs, shown in Fig. 1 along with crossed ladder diagrams. The original calculation is due to Polkinghorne [8,9]. It is also very useful to know that we can reconstruct the Regge behavior of the ladder sum from consideration of the s-channel discontinuities in the diagrams, where the relevant discontinuities are those where the cut lines are the rungs of the ladder, as in Fig. 2. In the cut analysis, it is required that all the ladder rungs correspond to on-shell modes, so this fact needs to be accommodated in the mode expansion.

Our analysis will start with the mode expansion for the scalar box diagram, the first diagram in Fig. 3. Along the way we will resolve a paradox that exists in the usual method of regions treatment of the box. In [4] Smirnov demonstrates how the box diagram can be reconstructed by the use of collinear modes for the vertical legs of the ladder, although an extra "analytic regularization" in which the propagators are modified is required. Indeed, we will also find this result with our regularization. However, when the legs are collinear modes, at least one of the horizontal rungs of the box must be a hard mode which is far of shell. (We will review the terminology and kinematics in more detail below.) By unitarity, the off-shell mode should not be able to produce the imaginary part of the box diagram. However, we will show that the imaginary part arises from an overlap

[*]donoghue@physics.umass.edu
[†]bmahmoud@physics.umass.edu
[‡]ovanesyan@umass.edu

[1]For more on the relation of this model to Regge behavior in QCD, see the book by Forshaw and Ross [7]. In this paper we will refer to the full theory as QCD and the effective theory alternately as SCET without Glauber modes or $SCET_G$ with them.

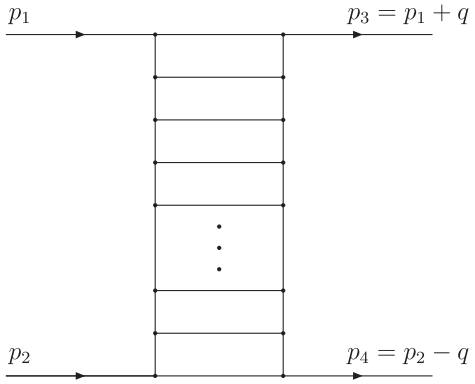

FIG. 1. The ladder graphs.

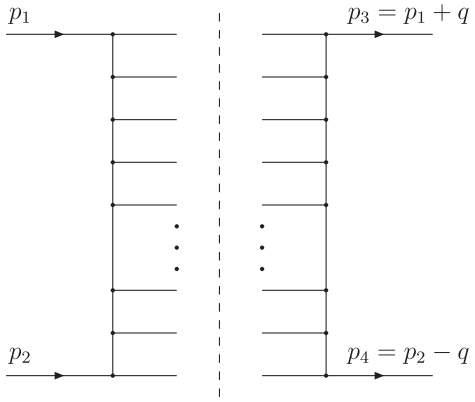

FIG. 2. The cut ladder graphs.

region which the collinear mode shares with Glauber exchange. By removing the overlap, the box can be reformulated in a version of SCET including the Glauber mode, $\mathrm{SCET_G}$, in which case the horizontal rung is in fact an on-shell (collinear) mode. The need to include Glauber modes in SCET has been shown by [10] (see also [11]); they have been shown to be important in the context of jets in a medium [12], and the relevance of these modes for Regge physics was first shown in [13].

The plan of this paper involves a brief overview of Regge behavior in Sec. 2, and of SCET kinematics in Sec. 3. Then in Sec. 4 (along with Appendix A) we provide a detailed treatment of the box diagram, paying particular attention to the overlap regions between modes and demonstrating the importance of the Glauber mode. Section 5 treats the two-loop ladder graph and shows how to count the modes and match to the full theory. This is continued to higher orders in Secs. 6 and 7. A conclusion summarizes what has been accomplished. While this paper was being finalized, an important related work by Fleming was released [14], and we also discuss the relation of our work to his in the conclusion. Three appendices provide some relevant technical details.

II. REGGE BEHAVIOR IN FIELD THEORY

For the purposes of this paper we will refer to Regge behavior as the dependence of the scattering amplitude on a power of the center-of-mass energy

$$\mathcal{M}_{\mathrm{QCD}} \sim s^{\alpha(t)} \tag{2}$$

in the limit $s \to \infty$, t fixed. The Regge exponent $\alpha(t)$ is dynamically generated through loop diagrams. At each order in perturbation theory, the loops generate logs, but in this kinematic region the logs exponentiate into a power. In general one finds

$$\mathcal{M}_{\mathrm{QCD}} \sim a_0 s^a \sum_{n=0}^{\infty} \frac{\beta^n(t)}{n!} \ln^n s + \cdots \to a_0 s^{a+\beta(t)} + \cdots, \tag{3}$$

where we have allowed an extra possible overall factor of s^a to the amplitude. (In our example $a = -1$.) It is this conversion of logs into powers that makes the phenomenon important for phenomenology. In real QCD one sees a variety of Regge exponents depending on the quantum numbers, including the Pomeron with $\alpha(0) \sim 1$.

Polkinghorne [8] was the first to show how this behavior emerges in a field theory, using a massive scalar field with the ϕ^3 interaction of Eq. (1). Although the ladder diagrams cannot be calculated completely, the leading high energy behavior emerges from a corner of the Feynman parameter integration and this corner can be analyzed and summed. For example, the direct box diagram shown in Fig. 3 after momentum integration becomes

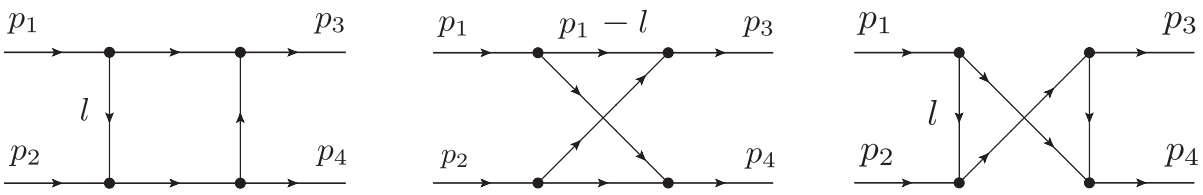

FIG. 3. One-loop Feynman diagrams with boxlike topology. We only show one internal momentum enough to clarify our conventions. The graphs represent the (s, t), (u, t), and (s, u) channels respectively. The last graph is suppressed by t/s compared to the first two.

$$i\mathcal{M}^{\rm box}_{\rm QCD} = i\frac{g^4}{16\pi^2}\int dx_1 dx_2 dy_1 dy_2 \frac{\delta(1-x_1-x_2-y_1-y_2)}{[x_1x_2 s + y_1y_2 t - m^2(1-(x_1+x_2)(y_1+y_2))]^2} \tag{4}$$

where x_1, x_2 are the Feynman parameters associated with the horizontal lines (rungs) in the diagram and y_1, y_2 are associated with the vertical lines (legs). It is clear from this that the amplitude falls as $1/s^2$ at large s, except for the region of integrations where x_1 and/or x_2 are close to zero. Polkinghorne noted that when only one of $x_{1,2}$ is small, the integrated amplitude falls as $1/s$, but when both of the parameters are small there is an extra logarithmic factor of $\ln(-s)$. In this corner the residual dependence on $x_{1,2}$ can be neglected and the result is

$$i\mathcal{M}^{\rm box}_{\rm QCD} = ig^2\beta(t)\frac{1}{-s}\ln(-s) \tag{5}$$

with $s = s + i0$ and

$$\beta(t) = \frac{g^2}{16\pi^2}\int dy_1 dy_2 \frac{\delta(1-y_1-y_2)}{[m^2 - y_1y_2 t]} = \frac{g^2}{4\pi}\int \frac{d^2\boldsymbol{l}_\perp}{(2\pi)^2}\frac{1}{[\boldsymbol{l}_\perp^2 + m^2][(\boldsymbol{l}_\perp+\boldsymbol{q}_\perp)^2 + m^2]}. \tag{6}$$

Note that the exponent depends on the transverse momenta only—the longitudinal components have been integrated out. The crossed-box diagram is obtained by the substitution $s \to u$, and since $s \gg -t, m^2$ we have $u \approx -s$. The sum of the box and crossed box then becomes

$$\mathcal{M}^{\rm box+crossed}_{\rm QCD} = -g^2\beta(t)\left[\frac{1}{s}\ln(-s) + \frac{1}{-s}\ln(s)\right] = \frac{i\pi}{s}g^2\beta(t). \tag{7}$$

This is the $n = 0$ term in the Regge sum of Eq. (3). In this case, we see that the result emerges entirely from the s-channel cut with both horizontal rungs being on shell.

The rest of the ladder sum is done in the same way. The important region in the integration is the corner where all the Feynman parameters associated with the horizontal rungs becomes small. In this corner the correct $\ln^n(-s)$ behavior arises and the sum yields the Regge form with amplitude and exponent being given by

$$a_0 = \frac{i\pi}{s}g^2\beta(t) \quad \text{and} \quad \alpha(t) = -1 + \beta(t). \tag{8}$$

In real QCD, the situation is somewhat more complicated, but follows the same kinematic rules. Within perturbative QCD, this has been demonstrated by Balitsky, Fadin, Kuraev, and Lipatov (BFKL) [15] and in related work [16].

III. KINEMATICS AND NOTATION

We consider the binary scattering of particles with momenta p_1 and p_2, while the outgoing particles carry momenta p_3 and p_4. The momentum transfer is defined as $q = p_3 - p_1$. We work in the center-of-mass frame and use light-cone coordinates requiring the introduction of two independent null vectors which read

$$n^\mu = (1,0,0,1), \qquad \bar{n}^\mu = (1,0,0,-1), \qquad n\cdot\bar{n} = 2. \tag{9}$$

Hence, four momenta are decomposed as follows:

$$p^\mu = p^+\frac{\bar{n}^\mu}{2} + p^-\frac{n^\mu}{2} + \boldsymbol{p}_\perp, \qquad p^+ \equiv p\cdot n, \qquad p^- \equiv p\cdot\bar{n}, \qquad \boldsymbol{p}_\perp\cdot n = \boldsymbol{p}_\perp\cdot\bar{n} = 0. \tag{10}$$

For later convenience, we note the following identity:

$$\mathrm{d}^4 l = \frac{1}{2}\mathrm{d}l^+\mathrm{d}l^-\mathrm{d}^2\boldsymbol{l}_\perp. \tag{11}$$

Regge physics is concerned with the kinematical limit

$$s \to \infty, \qquad -t, m^2 \ll s \tag{12}$$

where $s = (p_1+p_2)^2$ and $t = q^2$ are the usual Mandelstam variables. The small parameter required for employing the method of regions (SCET) then reads

$$\lambda = \sqrt{\frac{-t}{s}}. \tag{13}$$

All external particles are treated as massless and on shell, in particular $p_i^2 = 0$. Note that the scattering of two high energy on-shell particles, one in the n direction and the other in the $\bar{n}$ always involves an exchange in the so-called Glauber region. This can be readily seen from the on-shell conditions

$$p_3^2 = 0 = (p_1+q)^2 = 0 + p_1^- q^+ + t$$
$$p_4^2 = 0 = (p_2-q)^2 = 0 - p_2^+ q^- + t. \tag{14}$$

Because p_1^-, $p_2^+ \sim \sqrt{s}$, this forces q to scale as $q \sim \sqrt{s}(\lambda^2,\lambda^2,\lambda)$ in the $(+,-,\perp)$ directions. The Glauber region is characterized by having momentum dominantly in the transverse direction. The overall momentum transfer of Regge exchange is Glauber-like. In addition, one can include modes in the mode expansion which correspond to Glauber kinematics. Such modes are always off shell; thus,

in the effective theory language they can be treated as an effective potential.

There is an array of possibilities in the choice of infrared regulators for our calculation. Among them is the analytic regulator used in [4], off shellness of external momenta $p_i^2 \neq 0$, or internal masses $m_i \neq 0$. If one uses off shellness as a regulator with vanishing internal masses within the loop, one finds that the modes in the effective theory or method of regions are not regularized in four dimensions. Hence, off shellness by itself fails to regulate the infrared behavior of the theory and one needs to add a dimensional regulator in order to regulate the infrared divergences.

In this paper we regulate the infrared through the use of an internal mass for each internal line in any graph, keeping the external four-vectors on shell with zero invariant mass. This fully controls the infrared region. For the leading high energy behavior the answer is the same if one uses massive external four-vectors with the same m^2 as in the original Polkinghorne calculation.

In the remainder of this paper we study how Regge behavior in the toy scalar theory arises in the effective theory. It has to be noted however that this paper is lacking a complete consistent effective theory derivation of Regge behavior for QCD. This understanding is very important and is beyond the scope of this paper. What this paper contains is the method of region derivation of Regge behavior and is supposed to pave the way into a consistent effective field theory (EFT) formulation of Regge physics. The modes that we consider in the method of regions are those of SCET and SCET_G.

For concreteness we present the Lagrangians of effective theories for the toy scalar QCD theory. Pulling out the label momentum from the scalar field $\phi(x) = \sum_{\tilde{p}} e^{-i\tilde{p}\cdot x}\phi_{n,p}$, where $\tilde{p} = (0, \bar{n}\cdot p, p_\perp)$, we get[2]

$$\begin{aligned}\mathcal{L}_{\text{SCET}} &= \sum_n \mathcal{L}_c^{(n)} + \mathcal{L}_s + \mathcal{L}_{cs},\\ \mathcal{L}_c^{(n)} &= \sum_{\tilde{p}} \frac{1}{2}\left[|\partial_\mu \phi_{n,p}|^2 - m^2|\phi_{n,p}|^2\right]\\ &\quad + \frac{g}{3!}\sum_{\tilde{p}_1,\tilde{p}_2,\tilde{p}_3} e^{-i(\tilde{p}_1-\tilde{p}_2-\tilde{p}_3)\cdot x}\phi_{n,p_1}\phi^\dagger_{n,p_2}\phi^\dagger_{n,p_3}.\end{aligned} \tag{15}$$

We only specify the collinear sector of SCET because for reasons that are spelled out in the next section we do not consider graphs with soft gluons. The Lagrangian of SCET_G has an additional four-point interaction where the Glauber gluon is integrated out:

$$\begin{aligned}\mathcal{L}_{\text{SCET}_\text{G}} &= \mathcal{L}_{\text{SCET}} - \sum_{\tilde{p}_1,\tilde{p}_2,\tilde{p}_3,\tilde{p}_4} \frac{g^2 e^{-i(\tilde{p}_1+\tilde{p}_2-\tilde{p}_3-\tilde{p}_4)\cdot x}}{(\boldsymbol{p}_{1\perp}-\boldsymbol{p}_{3\perp})^2}\\ &\quad \times \phi_{n,p_1}\phi_{\bar{n},p_2}\phi^\dagger_{n,p_3}\phi^\dagger_{\bar{n},p_4}.\end{aligned} \tag{16}$$

[2]For real field $\phi(x)$ we have $\phi_{n,p} \equiv \phi^\dagger_{n,-p}$.

In what follows we identify the contributions to the Regge behavior using the method of regions by keeping modes of either of the two effective theories mentioned above. We emphasize that SCET and SCET_G in our case are understood in the sense of the toy theory and should not be confused with effective theories for real QCD like Ref. [1] and an effective theory for jets in medium [12].

IV. ONE-LOOP BOX

In this section we calculate the one-loop $\mathcal{O}(g^4)$ contribution to Regge physics of the binary scattering explained above. We start off by computing the appropriate graphs in the full theory and then repeat the calculation using the method of regions to isolate the modes responsible for Regge behavior. The graphs at the one-loop level which concern Regge physics are the ones with boxlike topology shown in Fig. 3. In fact, the last graph has a suppressed leading behavior (by a power of s) compared to the first two and thus we neglect this graph all together. To fix the nomenclature, we refer to the first graph as the "direct box" and the second as the "crossed box."

A. The box diagram in the full theory

The full Regge amplitude is simply obtained by summing the two graphs to find

$$\begin{aligned}\mathcal{M}^{(1)}_{\text{QCD}} &= (-i)g^4\frac{1}{2}\int\frac{d^4l}{(2\pi)^4}\frac{1}{(l^2-m^2+i0)((l+q)^2-m^2+i0)}\\ &\quad\times\left(\frac{1}{(l-p_1)^2-m^2+i0}+\frac{1}{(l+p_3)^2-m^2+i0}\right)\\ &\quad\times\left(\frac{1}{(l+p_2)^2-m^2+i0}+\frac{1}{(l-p_4)^2-m^2+i0}\right).\end{aligned} \tag{17}$$

In the above expression we combined the graphs after symmetrizing each under the interchange $l\leftrightarrow -(l+q)$, and hence the factor of half. This does not prove useful for the full theory calculation but considerably simplifies the calculation in the method of regions. The intermediate steps of the computation are rather complicated and we move the details to Appendix A but the final result in the limit $s \gg -t, m^2$ takes the simple form

$$\mathcal{M}^{(1)}_{\text{QCD}} = \frac{i\pi g^2\beta(t)}{s}, \tag{18}$$

where $\beta(t)$ is defined in Eq. (6) and explicitly reads

$$\begin{aligned}\beta(t) &= \frac{g^2}{8\pi^2(-t)\chi(t)}\ln\frac{\chi(t)+1}{\chi(t)-1}, \quad \text{and}\\ \chi(t) &= \sqrt{1-\frac{4m^2}{t}} > 1.\end{aligned} \tag{19}$$

To arrive at this expression we have kept all the finite terms in the expansion t/s, m^2/s and only dropped power-suppressed ones.

Below we concentrate on the method of regions for the calculation of the Regge behavior using the modes of two effective theories, SCET and SCET_G. Usually the power counting and pinch analysis are used to determine which modes to include into the method of region. For the massive one-loop QCD box integral such analysis identifies only two regions: collinear and anticollinear. The ultrasoft mode $(\lambda^2, \lambda^2, \lambda^2)$ is power suppressed and the soft mode $(\lambda, \lambda, \lambda)$ is leading order but is not pinched. As is well known, the Glauber mode is not pinched for the box topology. This mode only becomes pinched in the pentagon topology. Based on these facts we first consider only the two collinear graphs, which we refer to as the modes of SCET (in this case all leading modes of SCET_I-EFT with collinear and ultrasoft particles). As will be mentioned later, there is a paradox in reproducing the Regge behavior with only these two modes, because of the imaginary part of the combined result and unitarity issues. As we will see below, including the Glauber mode resolves this issue, and our second EFT of choice is SCET_G, where again only leading graphs of SCET_I are considered plus Glauber region.

B. The box diagram in SCET without Glauber modes

Using the modes of SCET we get two leading graphs, when the loop momentum is either n collinear or $\bar{n}$ collinear. An ultrasoft loop momentum $(\lambda^2, \lambda^2, \lambda^2)$ on the other hand is power suppressed because m^2 scales as λ^2. With some details in Appendix A, we find that both n- and $\bar{n}$-collinear graphs shown in Fig. 4 are equal

$$\mathcal{M}_n^{(1)} = \mathcal{M}_{\bar{n}}^{(1)} = \mathcal{M}_{\text{QCD}}^{(1)}. \tag{20}$$

Hence, summing both contributions gives a result twice as big as the full theory. It turns out that the overlap contribution of these two modes is nonvanishing and must be taken into account in order to correctly reproduce the full theory result

$$\mathcal{M}_{n/\bar{n}}^{(1)} = \mathcal{M}_{\text{QCD}}^{(1)}. \tag{21}$$

We derive a master formula in Appendix C that takes into account correct subtraction terms when combining N momentum regions in the method of regions. Applying it for two modes, we reproduce the QCD result

$$\mathcal{M}_{\text{SCET}}^{(1)} = \mathcal{M}_n^{(1)} + \mathcal{M}_{\bar{n}}^{(1)} - \mathcal{M}_{n/\bar{n}}^{(1)} = \mathcal{M}_{\text{QCD}}^{(1)}. \tag{22}$$

We have found that using the modes of SCET we recover the full QCD loop integral. This should not be surprising since for the box integral the pinch analysis leads to no Glauber pinch [10,17], i.e., modes of SCET are sufficient. However, there is something strange with this result. Indeed the full answer for the QCD integral (defined by including the crossed-box graph) is purely imaginary; see Eq. (18). This imaginary part can be obtained from the discontinuity of the direct box integral. This discontinuity comes from on-shell intermediate states; however, both collinear graphs $\mathcal{M}_n$ and $\mathcal{M}_{\bar{n}}$ have one propagator far off shell. Thus, the imaginary part should come from the subregion of these two modes and is contained in a different kinematic region. In the book [4], the one-loop box integral with the Regge kinematics was calculated using an analytic regulator. It was found that the box integral is recovered from two collinear graphs, similarly to our finding in this section with our regularization. Note, that with their regulator the overlap contribution vanishes and does not play role. Thus, the same comment that the imaginary part of the box graph is coming from a different kinematic region and is outside of collinear graphs holds for the calculation in [4]. Below we repeat the one-loop calculation with our regulator by including all the modes of SCET_G with their overlaps and this paradox is resolved.

C. The problem of the imaginary part

The imaginary part of the collinear amplitudes hints that we are missing insight into Regge physics. The imaginary part of the full theory should not be expected to come from collinear exchange. In simple words, this is because the collinear graphs indeed have one intermediate state off shell. To elucidate this point, we directly employ Cutkosky rule to compute the imaginary part of the direct-box graph. Hence,

$$\text{Im}\mathcal{M}_{\text{QCD}}^{(1)} = \frac{g^4}{8\pi^2}\int d^4 l \frac{\delta_+((p_1-l)^2-m^2)\delta_+((l+p_2)^2-m^2)}{(l^2-m^2)((l+q)^2-m^2)} \tag{23}$$

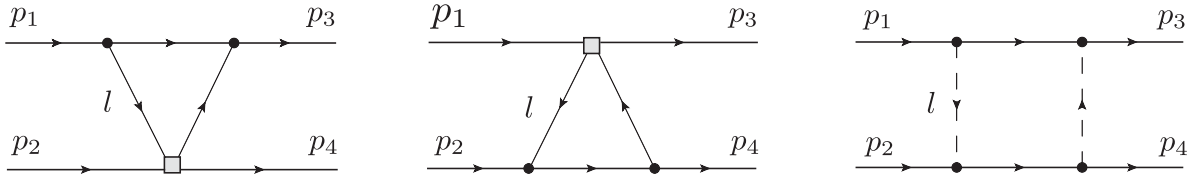

FIG. 4. Direct-box diagrams in SCET_G. The box represents an off-shell propagator and the dashed lines refer to Glauber modes. The momentum routing is identical to the box in Fig. 3. In SCET, only the first two graphs appear.

where $\delta_+(p^2-m^2)=\delta(p^2-m^2)\Theta(p^0)$. This integral is easily rewritten as

$$\mathrm{Im}\mathcal{M}^{(1)}_{\mathrm{QCD}}=\frac{g^4}{16\pi^2\sqrt{s}}\int d^4l \times\frac{\delta((p_1-l)^2-m^2)\delta(l^0)}{\sqrt{s}(l^0-l_z)(\sqrt{s}(l^0-l_z)+q^2-2\vec{l}\cdot\vec{q})}. \quad (24)$$

Notice that $q^0=0$ since we work in the center-of-mass frame. The integral over l^0 is readily done to absorb the second delta function and forces $l^0=0$. This is very interesting because this means that $l^\pm=\mp l_z$, which shows that the mode responsible for generating the leading Regge behavior ought to have longitudinal components of equal scaling, a condition clearly violated by collinear modes. We continue the calculation by performing the l_z integral where a quadratic form appears in the argument of the delta function with the following roots:

$$l_z^\pm=\frac{\sqrt{s}}{2}\left(1\pm\sqrt{1-\frac{4\Delta}{s}}\right),\qquad \Delta=\boldsymbol{l}_\perp^2+m^2. \quad (25)$$

The "+/−" refers to large/small root, respectively. Clearly, the transverse integral has to be constrained since $4\Delta\le s$ for $l_z^\pm$ to be real. The large root yields a result proportional to $1/s^2$, and hence is power suppressed. On the other hand, the small root can be Taylor expanded

$$l_z^-=\frac{\Delta}{\sqrt{s}}\left(1+\frac{\Delta}{s}+\cdots\right). \quad (26)$$

The first term in the expansion yields the leading result in the Regge limit, and hence $l_z^-\approx\Delta/\sqrt{s}$. This is the second piece of information we need to pin down the Regge mode; it has an excess in the transverse direction identical to the momentum transfer. We conclude that Glauber scaling $l\sim\sqrt{s}(\lambda^2,\lambda^2,\lambda)$ is genuinely responsible for Regge behavior. Finally, the result agrees with the full calculation

$$\mathrm{Im}\mathcal{M}^{(1)}_{\mathrm{QCD}}=\frac{\pi g^2\beta(t)}{s}. \quad (27)$$

D. The box diagram in SCET$_{\mathrm{G}}$

In soft collinear effective theory with Glauber modes an additional graph appears where the loop momentum is that of Glauber scaling $l(\lambda^2,\lambda^2,\lambda)$. With details provided in Appendix A, the box integral in this momentum region is equal to

$$\mathcal{M}^{(1)}_G=\mathcal{M}^{(1)}_{\mathrm{QCD}}. \quad (28)$$

When adding the Glauber as an independent mode, overlaps with collinear modes must be taken into account, we calculate these in Appendix A. The result is

$$\mathcal{M}^{(1)}_{n/G}=\mathcal{M}^{(1)}_{\bar n/G}=\mathcal{M}^{(1)}_{n/\bar n/G}=\mathcal{M}^{(1)}_{G}=\mathcal{M}^{(1)}_{\mathrm{QCD}}. \quad (29)$$

Our calculation indicates that the imaginary part of the full theory is coming precisely from the Glauber region (at the one-loop order). In other words, the matching in SCET$_{\mathrm{G}}$ after all zero-bin (overlap) subtractions gives the same result as just the Glauber mode

$$\mathcal{M}^{(1)}_{\mathrm{SCET_G}}=\mathcal{M}^{(1)}_{n}+\mathcal{M}^{(1)}_{\bar n}+\mathcal{M}^{\mathrm{box}}_{G}-\mathcal{M}^{(1)}_{n/\bar n}-\mathcal{M}^{(1)}_{n/G} -\mathcal{M}^{(1)}_{\bar n/G}+\mathcal{M}^{(1)}_{n/\bar n/G}=\mathcal{M}^{(1)}_{G}=\mathcal{M}^{(1)}_{\mathrm{QCD}}. \quad (30)$$

As is well known from factorization proofs of the Drell-Yan process, the Glauber region is not pinched for the box topology [17], (see also [10]). Thus, it is no surprise that we get the same answer in SCET$_{\mathrm{G}}$ as in SCET. When one uses the modes of SCET, the collinear integrals each contain at least one of the intermediate propagators off shell; thus, the imaginary part[3] ought to come from a subregion inside them. Our calculation above precisely shows that the correct momentum region for the full box integral in the Regge kinematics (when the direct and crossed box are added) is the *Glauber* region. What we mean by this is that the QCD box integral with the crossed box added at one loop can be reproduced by a single Glauber mode, which does not violate unitarity. As one adds the collinear graphs and Glauber one together, the interpretation can be made that the true collinear mode obtained from the naive collinear mode after zero-bin subtraction becomes purely real (as it should be due to unitarity) and cancels out between box and crossed box. Thus, we resolve the paradox of the imaginary part coming from collinear graphs. We will see below in this paper that this generalizes straightforwardly to higher orders in perturbation theory.

E. The imaginary part via the Cutkosky rule

For completeness and as a prelude to the next section, we directly use the Cutkosky rule to recalculate the imaginary part albeit taking the loop momentum in the Glauber region. The computation is very simple and the correct result is obtained effortlessly. Expanding the integrand of (23) and explicitly employing light-cone coordinates

$$\mathrm{Im}\mathcal{M}^{(1)}_{G}=\frac{g^4}{16\pi^2}\int \mathrm{d}^2\boldsymbol{l}_\perp \mathrm{d}l^+\mathrm{d}l^- \times\frac{\delta(-\boldsymbol{l}_\perp^2-\sqrt{s}l^+-m^2)\delta(-\boldsymbol{l}_\perp^2+\sqrt{s}l^--m^2)}{(\boldsymbol{l}_\perp^2+m^2)((\boldsymbol{l}_\perp+\boldsymbol{q}_\perp)^2+m^2)}. \quad (31)$$

The step functions are automatically satisfied. The longitudinal momenta integrals are used trivially to absorb the delta functions and we find

[3]Note that the entire one-loop expression of the QCD amplitude is imaginary; see Eq. (18).

$$\mathrm{Im}\mathcal{M}_G^{(1)} = \frac{\pi g^2 \beta(t)}{s}. \tag{32}$$

As previously mentioned, the kinematic exercise of Eq. (14) combined with the Cutkosky rule for the on-shell intermediate states of the box diagram requires that the exchanged mode be in the Glauber region.[4]

V. TWO-LOOP LADDER

We saw at one loop that the underlying physics behind Regge behavior is the imaginary part of the direct-box graph caused by the s-channel discontinuity. This picture is valid at any loop order as confirmed by the Polkinghorne analysis [8]. Hence, we confine the subsequent discussion to only the imaginary part of higher loop graphs that contribute to Regge physics, i.e., ladder graphs.

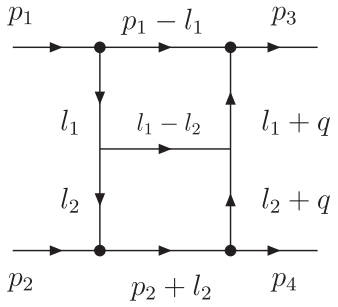

FIG. 5. Two-loop direct graph in full theory (QCD).

A. The double box ladder in the full theory

The imaginary part of the two-loop ladder graph shown in Fig. 5 is given by

$$\mathrm{Im}\mathcal{M}_{\mathrm{QCD}}^{(2)} = \frac{g^6}{64\pi^5}\int d^4l_1 d^4l_2 \frac{\delta_+[(p_1-l_1)^2-m^2]\delta_+[(l_1-l_2)^2-m^2]\delta_+[(p_2+l_2)^2-m^2]}{(l_1^2-m^2)(l_2^2-m^2)((l_1+q)^2-m^2)((l_2+q)^2-m^2)}, \tag{33}$$

where δ_+ is defined as before. This integral has extensively been studied before with the result

$$\mathrm{Im}\mathcal{M}_{\mathrm{QCD}}^{(2)} \approx \frac{\pi g^2 \beta^2(t)}{s}\ln s. \tag{34}$$

For example, see the derivation in [7,13], where it is shown that the leading region is the so-called strongly ordered one. The formula above contains the leading logarithm as $s \to \infty$. There are finite terms beyond this logarithm that are the same order in the t/s expansion and thus are expected to be captured by the method of regions or the mode expansion. For this reason we derived such terms in Appendix B, but for simplicity we have set $t = 0$. This leads to a finite answer in four dimensions because our massive theory is infrared safe. The result is

$$\mathrm{Im}\mathcal{M}_{\mathrm{QCD}}^{(2)}(t=0) = \frac{g^6}{256\pi^5}\int d^2\boldsymbol{l}_{1\perp} d^2\boldsymbol{l}_{2\perp} \frac{1}{s(\Delta_1\Delta_2)^2}\left[\ln\frac{s}{\Delta_{12}} - 2\right]\theta(s - (\sqrt{\Delta_1}+\sqrt{\Delta_2}+\sqrt{\Delta_{12}})^2). \tag{35}$$

In the equation above we have made the following definitions in terms of transverse momenta:

$$\Delta_1 = \boldsymbol{l}_{1\perp}^2 + m^2, \qquad \Delta_2 = \boldsymbol{l}_{2\perp}^2 + m^2, \qquad \Delta_{12} = (\boldsymbol{l}_{1\perp} - \boldsymbol{l}_{2\perp})^2 + m^2. \tag{36}$$

B. Matching in SCET$_{\mathrm{G}}$

So far we have learned from the one-loop calculation that the correct momentum region to understand the Regge behavior is when all intermediate states are on shell. The only way to do this at two loops is one of the three possibilities (l_1, l_2) is (n, G), $(G, \bar{n})$, (G, G). Power counting the mode integrals shows that (G, G) must be suppressed, due to the higher power of the momentum-space volume factor $d^4l_G \sim \lambda^6$ as opposed to $d^4l_{\mathrm{coll}} \sim \lambda^4$. The fact that there are two leading modes (shown in Fig. 6) means that their overlap must be taken into account. The first of our modes equals to

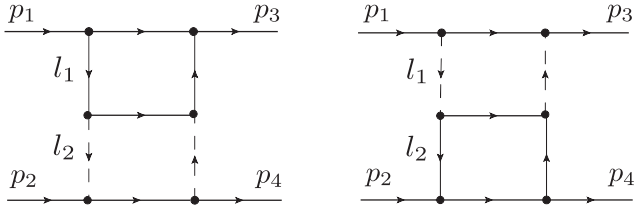

FIG. 6. Two-loop graphs in SCET$_{\mathrm{G}}$. From left to right these amplitudes are $\mathcal{M}_{nG}$, $\mathcal{M}_{G\bar{n}}$. All other two-loop graphs in the method of regions, for example $\mathcal{M}_{\bar{n}n}$, are power suppressed or lead to intermediate off-shell propagators, such as $\mathcal{M}_{nn}$.

[4]We note that the analytic regulator used in [4] sets the Glauber region to zero. It is then not consistent with the Cutkosky rule and we view this as a disadvantage of this regulator.

$$\mathrm{Im}\mathcal{M}^{(2)}_{nG} = \frac{g^6}{64\pi^5}\int d^4l_1 d^4l_2 \frac{\delta_+[(-l_1^+)(\sqrt{s}-l_1^-)-\Delta_1]\delta_+[(l_1^+-l_2^+)l_1^- - \Delta_{12}]\delta_+[\sqrt{s}l_2^- - \Delta_2]\theta(\sqrt{s}+l_2^+)}{(l_1^+l_1^- - \Delta_1)(-\Delta_2)((l_1^+ + q^+)l_1^- - \Delta_{1q})(-\Delta_{2q})}, \tag{37}$$

where the theta function in each of the δ_+ that appear above is the *expanded* expression in the QCD integral. We note that with such strict manifest power counting the limits of integration on the l_1^- after the l_1^+, l_2^+, l_2^- integrals are performed using the delta functions are not regulated and lead to a divergent result. To overcome this shortcoming we restore the *unexpanded* theta function in the $\delta_+[(p_2+l_2)^2-m^2]$ present in QCD expression. We made this explicit by inserting $\theta(\sqrt{s}+l_2^+)$ in Eq. (39). This *ad hoc* solution would not be satisfactory for a consistent EFT description of Regge physics. A more rigorous and promising approach seems to be introducing a rapidity regulator in the EFT; see Ref. [18]. In Ref. [14], the Regge behavior was derived from using rapidity renormalization group techniques developed in [18]. This approach is being further developed in the ongoing work by Rothstein and Stewart [19].

In the equation above we made the following definitions:

$$\Delta_{1q} = (\boldsymbol{l}_{1\perp}+\boldsymbol{q}_\perp)^2 + m^2, \qquad \Delta_{2q} = (\boldsymbol{l}_{2\perp}+\boldsymbol{q}_\perp)^2 + m^2. \tag{38}$$

With details explained in Appendix B we derive the expression for this mode for arbitrary values of t:

$$\begin{aligned}\mathrm{Im}\mathcal{M}^{(2)}_{nG} = {}& \frac{g^6}{256\pi^5}\int d^2\boldsymbol{l}_{1\perp}\mathrm{d}^2\boldsymbol{l}_{2\perp}\frac{1}{s\Delta_1\Delta_2\Delta_{1q}\Delta_{2q}} \\ & \times\left[\ln\frac{s}{\Delta_{12}} + \frac{1}{2}\ln\frac{\Delta_{1q}}{\Delta_1} - \frac{\arctan U}{U}\right]\theta \\ & \times (s-(\sqrt{\Delta_{12}}+\sqrt{\Delta_1})^2),\end{aligned} \tag{39}$$

where

$$U = \sqrt{\frac{4\Delta_1\Delta_{1q}}{(t+\Delta_1+\Delta_{1q})^2} - 1}. \tag{40}$$

In the entire domain of integration over $\boldsymbol{l}_{1\perp}, \boldsymbol{l}_{2\perp}$ the value of $U > 0$ and the answer is well behaved. By the same argument as above it is clear that in the leading limit in the power expansion as $s\to\infty$ the theta function in Eq. (39) can be ignored. Taking the leading logarithmic limit of Eq. (39) we get

$$\mathrm{Im}\mathcal{M}^{(2)}_{nG} \approx \frac{\pi g^2\beta^2(t)}{s}\ln s. \tag{41}$$

The calculation of the second mode $(G,\bar{n})$ proceeds analogously and leads to the identical result:

$$\mathrm{Im}\mathcal{M}^{(2)}_{G\bar{n}} = \mathrm{Im}\mathcal{M}^{(2)}_{nG}. \tag{42}$$

The fact that both modes yield identical results can also be seen from the following change of variables in the loop integrals:

$$l_1^\pm \leftrightarrow -l_2^\mp, \qquad \boldsymbol{l}_{1\perp}\leftrightarrow\boldsymbol{l}_{2\perp}. \tag{43}$$

This change of variables transforms the integrand of the $(G,\bar{n})$ mode with the one of the (n,G) mode. Note that both modes that we considered reproduce exactly the leading Regge behavior of QCD, so if one adds them together the result is that of twice of QCD. We should remember from our one-loop computation that overlaps need to be included, and thus we proceed to calculate the $(nG, G\bar{n})$ overlap.

C. The Regge mode

Here, we show that the overlap is the generator of Regge physics. Expanding the integrand of (33) subsequently with the scaling of the modes nG and $G\bar{n}$, all propagators become transverse and factor out of the longitudinal integration

$$\mathrm{Im}\mathcal{M}^{(2)}_{nG/G\bar{n}} = \frac{g^6}{64\pi^5}\int d^4l_1 d^4l_2 \frac{\delta_+[(-l_1^+)\sqrt{s}-\Delta_1]\delta_+[(-l_2^+)l_1^- - \Delta_{12}]\delta_+[\sqrt{s}l_2^- - \Delta_2]\theta(\sqrt{s}-l_1^-)\theta(\sqrt{s}+l_2^+)}{(-\Delta_1)(-\Delta_2)(-\Delta_{1q})(-\Delta_{2q})}. \tag{44}$$

Note that the theta functions in δ_+ are also *expanded* in this momentum region and similarly to the nG mode considered above we inserted additional theta functions present in the full QCD expression that help regulate integrals. Using the delta functions yields

$$\bar{l}_1^+ = -\frac{\Delta_1}{\sqrt{s}}, \qquad \bar{l}_2^- = \frac{\Delta_2}{\sqrt{s}}, \qquad \bar{l}_2^+ = -\frac{\Delta_{12}}{l_2^+}. \tag{45}$$

As a result the overlap integral is equal to

$$\mathrm{Im}\mathcal{M}^{(2)}_{nG/G\bar{n}} = \frac{g^6}{256\pi^5}\frac{1}{s}\int d^2\boldsymbol{l}_1 d^2\boldsymbol{l}_2 \frac{1}{\Delta_1\Delta_2\Delta_{1q}\Delta_{2q}} I_{l_1^-}, \quad (46)$$

where

$$I_{l_1^-} = \int_{\Delta_{12}/\sqrt{s}}^{\sqrt{s}} \mathrm{d}l_1^- \frac{1}{l_1^-} = \ln\left(\frac{s}{\Delta_{12}}\right). \quad (47)$$

Thus, the overlap correctly captures the subregion $l_1^- \ll \sqrt{s}$ and thus the final result in the Regge limit reads

$$\mathrm{Im}\mathcal{M}^{(2)}_{nG/G\bar{n}} = \frac{\pi g^2\beta^2(t)}{s}\ln s. \quad (48)$$

This is same answer as in the Regge limit of QCD.

D. Combining the modes of $\mathrm{SCET_G}$

Combining all the modes in the effective theory under consideration, we get

$$\begin{aligned}\mathrm{Im}\mathcal{M}^{(2)}_{\mathrm{SCET_G}} &= \mathrm{Im}(\mathcal{M}^{(2)}_{nG} + \mathcal{M}^{(2)}_{G\bar{n}} - \mathcal{M}^{(2)}_{nG/G\bar{n}}) \\ &= \frac{g^6}{256\pi^5}\int d^2\boldsymbol{l}_{1\perp}\mathrm{d}^2\boldsymbol{l}_{2\perp}\frac{1}{s\Delta_1\Delta_2\Delta_{1q}\Delta_{2q}} \\ &\quad\times\left[\ln\frac{s}{\Delta_{12}} + \ln\frac{\Delta_{1q}}{\Delta_1} - 2\frac{\arctan U}{U}\right]. \quad (49)\end{aligned}$$

This combined answer reduced to the case $t = 0$ reproduces the QCD result exactly

$$\begin{aligned}\mathrm{Im}\mathcal{M}^{(2)}_{\mathrm{SCET_G}}(t=0) &= \frac{g^6}{256\pi^5}\int d^2\boldsymbol{l}_{1\perp}\mathrm{d}^2\boldsymbol{l}_{2\perp}\frac{1}{s(\Delta_1\Delta_2)^2} \\ &\quad\times\left[\ln\frac{s}{\Delta_{12}} - 2\right] \\ &= \mathrm{Im}\mathcal{M}^{(2)}_{\mathrm{QCD}}(t=0). \quad (50)\end{aligned}$$

It also reproduces the leading Regge behavior of the QCD integral for arbitrary t. The fact that the leading Regge behavior is present in both modes and in the overlap as well, simply means that the true region from which the leading logarithm is coming is the overlap region. This result must be intimately connected to the strong ordering in the leading Regge limit. Indeed, strong ordering is a very special region in the momentum space with the hierarchy of energies, and we argue that our observation that the leading mode is the overlap has the same roots. In the remaining sections we provide arguments why this conclusions persists to higher orders.

VI. THREE-LOOP LADDER

In this section, we demonstrate that the full overlap between all "on-shell" modes immediately yields the leading Regge behavior similar to the two-loop case. At three loops we find three leading modes: (n, n, G) $(n, G, \bar{n})$, $(G, \bar{n}, \bar{n})$. The imaginary part of the three-loop ladder is obtained via the Cutkosky rule and the expression is similar to (44). The three-fold overlap between the leading modes forces all the propagators to become transverse and factor out as before. A close look at the expansion of the arguments of the delta functions for this multiple overlap momentum region leads to

$$\begin{aligned}\mathrm{Im}\mathcal{M}^{(3)}_{nnG/nG\bar{n}/G\bar{n}\,\bar{n}} &= \frac{g^8}{512\pi^8}\int \mathrm{d}^4l_1\mathrm{d}^4l_2\mathrm{d}^4l_3\frac{\delta_+(-\sqrt{s}l_1^+ - \Delta_1)\delta_+(-l_1^-l_2^+ - \Delta_{12})\delta_+(-l_2^-l_3^+ - \Delta_{23})\delta_+(\sqrt{s}l_3^- - \Delta_3)}{\Delta_1\Delta_2\Delta_3\Delta_{1q}\Delta_{2q}\Delta_{3q}} \\ &= \frac{g^8}{512\pi^8}\frac{1}{2^3}\frac{1}{s}\int \mathrm{d}^2\boldsymbol{l}_{1\perp}\mathrm{d}^2\boldsymbol{l}_{2\perp}\mathrm{d}^2\boldsymbol{l}_{3\perp}\frac{1}{\Delta_1\Delta_2\Delta_3\Delta_{1q}\Delta_{2q}\Delta_{3q}} I_{l_1^-l_2^-}. \quad (51)\end{aligned}$$

Notice the nice feature that the appearance of Δ_i terms inside the δ functions follows from the consistent power counting of the multi-overlap region. We use the delta function to integrate over all plus components in addition to l_3^-, and the remaining nontrivial integrals read [5]

$$I_{l_1^-l_2^-} = \int_{\Delta/\sqrt{s}}^{\sqrt{s}}\frac{\mathrm{d}l_2^-}{l_2^-}\int_{l_2^-}^{\sqrt{s}}\frac{\mathrm{d}l_1^-}{l_1^-} \quad (52)$$

$$= \frac{1}{2}\ln^2\left(\frac{s}{\Delta}\right), \quad (53)$$

where Δ is a function of transverse momenta, but in the leading logarithmic approximation the answer does not depend on it. Finally, we get keeping only leading in the Regge limit term:

$$\mathrm{Im}\mathcal{M}^{(3)}_{nnG/nG\bar{n}/G\bar{n}\,\bar{n}} = \frac{\pi g^2\beta(t)^3}{s}\frac{\ln^2 s}{2}. \quad (54)$$

This matches the QCD result.

[5]The prescription adopted to get these limits of integration relies on *unexpanded* theta functions adopted from full the QCD expression. See the comment below Eq. (37) for a better way to regulate such loop integrals in the effective field theory.

VII. GENERALIZATION TO ALL ORDERS

From our explicit calculations at one- and two-loop orders it is easy to guess the answer for higher orders. We first guess the answer and then prove it further below. We expect that the true momentum region for the Regge kinematics at N-loop order is N leading graphs which are subset of $\mathrm{SCET_G}$ graphs with on-shell intermediate states. These are the graphs with a number of n-collinear gluons in the loops, a single Glauber gluon, and after it a number of $\bar{n}$-collinear momentum in the loops

$$\mathcal{M}^{(N)}_{n\ldots nG}, \qquad \mathcal{M}^{(N)}_{n\ldots nG\bar{n}\ldots\bar{n}}, \ldots \mathcal{M}^{(N)}_{G\bar{n}\ldots\bar{n}}. \tag{55}$$

Each of these amplitudes includes, by our definition, both the direct box and the crossed box. Each of these amplitudes reproduces the leading Regge behavior as $s \to \infty$ and also any overlap of any subset of these amplitudes reproduces the Regge behavior. Thus, once one combines all the modes, the answer is identical to only including a single mode which is the overlap of all N momentum regions.

In order to prove the above statements we use the strong ordering derivation to show that the arbitrary graph in the method of regions gives an identical result as a single loop integral in QCD. Consider, for example, an $\mathcal{M}^{(N)}_{G\bar{n}\ldots\bar{n}}$ graph. The loop momenta, l_i where $i = 1\ldots N$, scale as $(l_i^+, l_i^-, \boldsymbol{l}_{i\perp}) \sim (\lambda^2, \lambda^2, \lambda), (1, \lambda^2, \lambda), \ldots (1, \lambda^2, \lambda)$. Thus, the plus momentum satisfies $l_1^+ \sim \lambda^2 \ll l_2^+ \sim \cdots \sim l_k^+ \sim l_{k+1}^+ \sim \cdots \sim l_N^+ \sim 1$ and $l_1^- \sim l_2^- \sim \cdots \sim l_k^- \sim l_{k+1}^- \sim \cdots \sim l_N^- \sim \lambda^2$. Clearly the strong ordering region is a subregion of this region, since for the strong ordered region we have[6]

$$\begin{aligned} &|l_1^+| \ll |l_2^+| \cdots \ll |l_k^+| \ll |l_{k+1}^+| \ll \cdots \ll |l_N^+|, \\ &l_1^- \gg l_2^- \cdots \gg l_k^- \gg l_{k+1}^- \gg \cdots \gg l_N^-. \end{aligned} \tag{56}$$

Thus, repeating the usual strong ordering region derivation we would presumably get the same answer as in the full theory if we started to work on the graph $\mathcal{M}^{(N)}_{G\bar{n}\ldots\bar{n}}$. Similarly we can show that every other relevant graph is identical to one another, since they all contain the strong ordering region as their sub-region.

An analogous statement holds for any of the loop integrals involving Glauber gluons. These subsets of graphs are the only ones out of entire set that allow on-shell intermediate states. Our observation that the multi-overlap of these regions plays an important role has a simple interpretation. At N-loop order the single isolated momentum region that gives the leading Regge behavior is the multi-overlap of all on-shell modes $n\ldots nG/n\ldots nG\bar{n}\ldots\bar{n}/\ldots/G\bar{n}\ldots\bar{n}$. It is easy to verify by a straightforward calculation similar to what we did at three-loop order

$$\mathrm{Im}\mathcal{M}^{(N)}_{n\ldots nG/n\ldots nG\bar{n}\ldots\bar{n}/\ldots/G\bar{n}\ldots\bar{n}} = \frac{\pi g^2 \beta(t)}{s} \frac{(\beta(t)\ln s)^{N-1}}{(N-1)!}, \tag{57}$$

which reproduces the QCD Regge limit. In this section we showed that all leading modes have a strong ordering momentum region as their subregion, thus including only the multiple overlap of all these modes is sufficient and no surprise leads to the correct answer.

VIII. CONCLUSIONS

We have shown how one obtains Regge physics using the mode expansion of SCET. In the effective field theory, the key contributions come from overlap regions which must be carefully treated. The simplest and most consistent approach includes the Glauber modes of the effective field theory $\mathrm{SCET_G}$.

In the scalar theory that we discuss, the one-loop contribution that starts the Regge ladder sum comes from the imaginary part of the box diagram. The box diagram can be reproduced in an effective theory which includes only the hard and collinear modes. However, this comes at the cost of seemingly violating the unitarity property of field theory in that the imaginary part of the amplitude arises from a hard intermediate state which the effective theory says is far off shell. This result tells us that in fact the contribution comes from an overlap region with an on-shell mode. By including the exchange of Glauber modes in the description, we can again recover the full box diagram via the mode expansion. In this case, after accounting for the overlap regions, the imaginary part of the amplitude is properly obtained from the t-channel Glauber exchange with s-channel on-shell collinear modes.

At higher order the deconstruction of the various overlap regions continues, with a final result that is simple to state. Collinear modes provide many of the legs in the ladder sum, and all of the s-channel on-shell states. However, at any given loop order, a Glauber mode is responsible for the connection between the collinear n and $\bar{n}$ modes. We have explicitly demonstrated this at two loops, and provided an argument that this continues for all higher loops.

[6]Note, that in this expression all the "+" components are negative and all the "−" components are positive. This is imposed by the theta functions in the expression for the QCD cut graph.

As we were writing up our project, a related paper by Fleming showed how one can obtain the well-known BFKL equation from rapidity RGE in the effective theory [14]. In Fleming's calculation, the forward scattering matrix element which falls in the Glauber region is calculated to one-loop order and a rapidity divergent counterterm is determined. As a result the BFKL equation and the Regge behavior emerge from SCET with Glauber gluons. In our paper we also showed how Regge behavior emerges from SCET with Glauber gluons; however, we looked at it from a fixed order point of view by summing a series of graphs order by order in the perturbation theory. In doing so, we paid a special attention to the momentum region where the Regge behavior arises from and we concluded that the Glauber mode plays an important role to connect the n-collinear sector with the $\bar{n}$-collinear sector with keeping intermediate propagators on shell. The combined Regge mode we find is the mutual overlap of all such graphs at a given order and reproduces the Regge behavior. It should be noted that Fleming uses real QCD and works in the framework of $\mathrm{SCET_{II}}$ with Glaubers. In our work we only considered the modes of $\mathrm{SCET_I}$ with Glauber gluons added and used a toy scalar field theory. At the two-loop order we ran into divergent integrals, which we regulated in a certain way; see the discussion below Eq. (37). This allowed us to recover the correct Regge behavior from the method of regions. Using $\mathrm{SCET_{II}}$ with a rapidity regulator [18] seems to be one promising direction towards a consistent EFT formulation of the Regge behavior.

Neither this work nor [14] (nor the early work of [13]) is the final word on this subject. It is a common practice to apply SCET to resum Sudakov logarithms in high energy processes to very high orders in the logarithmic accuracy. The effective theory language is particularly efficient operationally. We hope that the results of this paper will guide the construction of a consistent EFT formulation of QCD that explains Regge behavior and allows the resummation of Regge logs similarly to existing techniques for Sudakov resummation. We need a technology that starts from the effective Lagrangian which allows a theorist to provide complete descriptions of processes including the usual SCET calculations but, in addition, include Regge contributions when appropriate. The good news is that we can now see that Regge physics can be compatible with the effective field theory. However, we do not yet have the complete technology to include such effects in a realistic calculation in a transparent and consistent fashion. From this work it follows that $\mathrm{SCET_G}$ is an obvious candidate for such an effective field theory. We will pursue such an approach in future work.

ACKNOWLEDGMENTS

We thank Iain Stewart, Martin Beneke, Thomas Becher, and Bernd Jantzen for useful conversations. J. F. D. thanks the Institut des Hautes Études Scientifiques, the Niels Bohr International Academy, and the University of Zurich for hospitality in early phases of this work. The work of J. F. D. and B. K. M. was supported in part by NSF Grants No. PHY-0855119 and No. PHY-1205986, and that of G. O. by DOE Grant No. DE-SC0011095.

APPENDIX A: THE BOX DIAGRAM AT ONE-LOOP ORDER

1. Full theory (QCD)

In this appendix, we list the calculational details of the box diagram in the full theory. We employ conventional Feynmann parametrization and integrate over the loop momentum to find within our regularization scheme

$$\mathcal{M}_{\mathrm{QCD}}^{\mathrm{box}} = \frac{g^4}{16\pi^2}\int_0^1 dx_1 dx_2 dy_1 dy_2 \frac{\delta(1-x_1-x_2-y_1-y_2)}{[x_1x_2s + y_1y_2t - m^2]^2} \tag{A1}$$

where it is understood that

$$s = s + i0, \qquad m^2 = m^2 - i0. \tag{A2}$$

The result can be expressed in terms of four basic integrals

$$\begin{aligned}\mathcal{M}_{\mathrm{QCD}}^{\mathrm{box}} = \frac{g^4}{16\pi^2}[&I_1(s,t,m^2) + I_2(s,t,m^2) \\ &+ I_1(t,s,m^2) + I_2(t,s,m^2)]\end{aligned} \tag{A3}$$

where

$$I_1(a,b,m^2) = \int_0^1 dy \frac{\ln(a(1-y)-by) - \ln(-by)}{y(1-y)ab - m^2a - y^2b^2},$$
$$I_2(a,b,m^2) = \int_0^1 dy \frac{\ln(m^2 - y(1-y)b) - \ln(m^2)}{y(1-y)ab - m^2a - y^2b^2}.$$

We list the results of the basic integrals in the Regge limit

$$
\begin{aligned}
I_1(s,t,m^2) &= \frac{1}{st\alpha}\left[\ln\left(\frac{s}{-t}\right)\ln\left(\frac{r_0^+}{r_0^-}\right)^2\right] \\
I_2(s,t,m^2) &= \frac{1}{st\alpha}\left[\ln\left(\frac{-t}{m^2}\right)\ln\left(\frac{r_0^+}{r_0^-}\right)^2 + \ln^2 l^+ - \ln^2(-l^-) - 2\ln(\alpha)\ln\left(\frac{-l^-}{l^+}\right) + 2\mathrm{Li}_2\left(\frac{-l^-}{\alpha}\right) - 2\mathrm{Li}_2\left(\frac{l^+}{\alpha}\right)\right] \\
I_1(t,s,m^2) &= \frac{1}{st\alpha}\left[\ln\left(\frac{s}{-t}\right)\ln\left(\frac{r_0^-}{r_0^+}\right)^2 + \mathrm{Li}_2\left(\frac{1}{r_0^-}\right) - \mathrm{Li}_2\left(\frac{1}{r_0^+}\right) - \mathrm{Li}_2\left(\frac{s}{-tr_0^-}\right) + \mathrm{Li}_2\left(\frac{s}{-tr_0^+}\right) + \mathrm{Li}_2\left(\frac{s}{tr_0^+}\right) - \mathrm{Li}_2\left(\frac{s}{tr_0^-}\right)\right] \\
I_2(t,s,m^2) &= \frac{1}{st\alpha}\left[-\ln\left(\frac{-s}{m^2}\right)\ln\left(\frac{r_0^-}{r_0^+}\right) + \mathrm{Li}_2\left(\frac{m^2}{m^2-tr_0^+}\right) - \mathrm{Li}_2\left(\frac{m^2}{m^2-tr_0^-}\right) + \mathrm{Li}_2\left(\frac{s}{tr_0^- - m^2}\right) - \mathrm{Li}_2\left(\frac{s}{tr_0^+ - m^2}\right)\right. \\
&\quad \left. - i\pi\left(\ln\left(\frac{-tr_0^+}{s}\right) - \ln\left(\frac{tr_0^-}{s}\right) + \ln\left(\frac{s}{m^2-tr_0^-}\right) - \ln\left(\frac{s}{m^2-tr_0^+}\right)\right) + \ln\left(\frac{m^2}{s}\right)\left(\ln\left(\frac{tr_0^+}{tr_0^+-m^2}\right) - \ln\left(\frac{tr_0^-}{tr_0^- - m^2}\right)\right)\right],
\end{aligned}
\tag{A4}
$$

where

$$
r_0^\pm = \frac{1}{2}(1 \pm \chi(t)), \qquad \chi(t) = \sqrt{1 - \frac{4m^2}{t}}. \tag{A5}
$$

We note the important simplification

$$
\ln\left(\frac{tr_0^\pm}{tr_0^\pm - m^2}\right) = \ln\left(\frac{1}{r_0^\pm}\right). \tag{A6}
$$

The crossed-box amplitude reads

$$
\mathcal{M}_{\mathrm{QCD}}^{\mathrm{cross}} = \frac{g^4}{16\pi^2}\int_0^1 dx_1 dx_2 dy_1 dy_2 \frac{\delta(1-x_1-x_2-y_1-y_2)}{[x_1x_2u + y_1y_2t - m^2]^2}. \tag{A7}
$$

In the Regge limit, $u \approx -s$ and hence

$$
\mathcal{M}_{\mathrm{QCD}}^{\mathrm{cross}} = \frac{g^4}{16\pi^2}[I_1(-s,t,m^2) + I_2(-s,t,m^2) + I_1(t,-s,m^2) + I_2(t,-s,m^2)]. \tag{A8}
$$

Upon summing both amplitudes, all terms cancel except the dilogarithms whose arguments approach infinity in the Regge limit. Those must be expanded and handled carefully, with the final result being

$$
\mathcal{M}_{\mathrm{QCD}} = \frac{ig^4}{8\pi st\chi(t)}\ln\left(\frac{\chi(t)-1}{\chi(t)+1}\right). \tag{A9}
$$

2. Modes in the EFT

Expanding the one-loop box integral in the n-collinear region we get

$$
\begin{aligned}
\mathcal{M}_n^{(1)} &= (-i)g^4\frac{1}{2}\int\frac{\mathrm{d}^4 l}{(2\pi)^4}\frac{1}{(l^2-m^2+i0)(l^-(l+q)^+ - (\boldsymbol{l}_\perp+\boldsymbol{q}_\perp)^2 - m^2 + i0)} \\
&\quad\times\left(\frac{1}{(l^- - \sqrt{s})l^+ - \boldsymbol{l}_\perp^2 - m^2 + i0} + \frac{1}{(l^- + \sqrt{s})(l+q)^+ - (\boldsymbol{l}_\perp+\boldsymbol{q}_\perp)^2 - m^2 + i0}\right) \\
&\quad\times\left(\frac{1}{\sqrt{s}l^- + i0} + \frac{1}{-\sqrt{s}l^- + i0}\right).
\end{aligned}
\tag{A10}
$$

This integral nicely collapses upon using the following identity:

$$\frac{1}{x+i\varepsilon}-\frac{1}{x-i\varepsilon}=-2i\pi\delta(x). \tag{A11}$$

The $\bar{n}$-collinear region yields an identical result, and we find[7]

$$\mathcal{M}_n^{(1)}=\mathcal{M}_{\bar{n}}^{(1)}=\mathcal{M}_{\mathrm{QCD}}^{(1)}. \tag{A12}$$

The overlap contribution of these two modes is nonvanishing and must be taken into account in order to correctly reproduce the full theory result

$$\begin{aligned}\mathcal{M}_{n/\bar{n}}^{(1)}=(-i)g^4\frac{1}{2}\int\frac{\mathrm{d}^4l}{(2\pi)^4}\frac{1}{(l^2-m^2+i0)(l^+l^--(\boldsymbol{l}_\perp+\boldsymbol{q}_\perp)^2-m^2+i0)}\\ \times\left(\frac{1}{-\sqrt{s}l^-+i0}+\frac{1}{\sqrt{s}l^-+i0}\right)\times\left(\frac{1}{\sqrt{s}l^++i0}+\frac{1}{-\sqrt{s}l^++i0}\right),\end{aligned} \tag{A13}$$

with the final result

$$\mathcal{M}_{n/\bar{n}}^{(1)}=\mathcal{M}_{\mathrm{QCD}}^{(1)}. \tag{A14}$$

In soft collinear effective theory with Glauber modes, an additional graph appears where the loop momentum is that of Glauber scaling $l(\lambda^2,\lambda^2,\lambda)$. The box integral in that momentum region reads

$$\begin{aligned}\mathcal{M}_G^{(1)}=(-i)g^4\frac{1}{2}\int\frac{\mathrm{d}^4l}{(\boldsymbol{l}_\perp^2+m^2-i0)((\boldsymbol{l}_\perp+\boldsymbol{q}_\perp)^2+m^2-i0)}\\ \times\left(\frac{1}{(-\boldsymbol{l}_\perp^2-\sqrt{s}l\cdot\bar{n}-m^2+i0)}+\frac{1}{(-\boldsymbol{l}_\perp^2+\sqrt{s}l\cdot\bar{n}-2\boldsymbol{l}_\perp\cdot\boldsymbol{q}_\perp-m^2+i0)}\right)\\ \times\left(\frac{1}{(-\boldsymbol{l}_\perp^2+\sqrt{s}l\cdot n-m^2+i0)}+\frac{1}{(-\boldsymbol{l}_\perp^2-\sqrt{s}l\cdot n-2\boldsymbol{l}_\perp\cdot\boldsymbol{q}_\perp-m^2+i0)}\right).\end{aligned} \tag{A15}$$

The integral is elementary and yields

$$\mathcal{M}_G^{(1)}=\mathcal{M}_{\mathrm{QCD}}^{(1)}. \tag{A16}$$

When adding the Glauber as an independent mode, overlaps with collinear modes must be taken into account

$$\begin{aligned}\mathcal{M}_{n/G}^{(1)}=(-i)g^4\frac{1}{2}\int\frac{\mathrm{d}^4l}{(\boldsymbol{l}_\perp^2+m^2-i0)((\boldsymbol{l}_\perp+\boldsymbol{q}_\perp)^2+m^2-i0)}\\ \times\left(\frac{1}{-\sqrt{s}l\cdot\bar{n}+i0}+\frac{1}{\sqrt{s}l\cdot\bar{n}+i0}\right)\\ \times\left(\frac{1}{(-\boldsymbol{l}_\perp^2+\sqrt{s}l\cdot n-m^2+i0)}+\frac{1}{(-\boldsymbol{l}_\perp^2-\sqrt{s}l\cdot n-2\boldsymbol{l}_\perp\cdot\boldsymbol{q}_\perp-m^2+i0)}\right),\end{aligned} \tag{A17}$$

[7]Note that from using Eq. (A11) it becomes clear that the true leading momentum region that contributes to this loop integral comes from a subregion where $l^-=0$. This is precisely the Glauber region, which is the subregion of the collinear region. Thus, the final answer, which is imaginary, arises from an on-shell intermediate mode, consistently with the unitarity. We thank our referee for emphasizing this point to us.

$$\mathcal{M}^{(1)}_{\bar{n}/G} = (-i)g^4\frac{1}{2}\int\frac{\mathrm{d}^4 l}{(\boldsymbol{l}_\perp^2+m^2-i0)((\boldsymbol{l}_\perp+\boldsymbol{q}_\perp)^2+m^2-i0)} \times\left(\frac{1}{(-\boldsymbol{l}_\perp^2-\sqrt{s}l\cdot\bar{n}-m^2+i0)}+\frac{1}{(-\boldsymbol{l}_\perp^2+\sqrt{s}l\cdot\bar{n}-2\boldsymbol{l}_\perp\cdot\boldsymbol{q}_\perp-m^2+i0)}\right) \times\left(\frac{1}{\sqrt{s}l\cdot n+i0}+\frac{1}{-\sqrt{s}l\cdot n+i0}\right), \tag{A18}$$

$$\mathcal{M}^{(1)}_{n/\bar{n}/G} = (-i)g^4\frac{1}{2}\int\frac{\mathrm{d}^4 l}{(\boldsymbol{l}_\perp^2+m^2-i0)((\boldsymbol{l}_\perp+\boldsymbol{q}_\perp)^2+m^2-i0)}\left(\frac{1}{-\sqrt{s}l\cdot\bar{n}+i0}+\frac{1}{+\sqrt{s}l\cdot\bar{n}+i0}\right) \times\left(\frac{1}{+\sqrt{s}l\cdot n+i0}+\frac{1}{(-\sqrt{s}l\cdot n+i0)}\right). \tag{A19}$$

The result of each is identical to the Glauber integral

$$\mathcal{M}^{(1)}_{n/G} = \mathcal{M}^{(1)}_{\bar{n}/G} = \mathcal{M}^{(1)}_{n/\bar{n}/G} = \mathcal{M}^{(1)}_{G} = \mathcal{M}^{(1)}_{\mathrm{QCD}}. \tag{A20}$$

APPENDIX B: THE LADDER DIAGRAM AT TWO-LOOP ORDER

1. Full theory (QCD)

Using Cutkosky's rules, the imaginary part of the two-loop ladder graph in the full theory (QCD) can be written as

$$\mathrm{Im}\mathcal{M}^{(2)}_{\mathrm{QCD}} = \frac{g^6}{64\pi^5}\int d^4l_1 d^4l_2\,\frac{\delta_+[(p_1-l_1)^2-m^2]\delta_+[(l_1-l_2)^2-m^2]\delta_+[(p_2+l_2)^2-m^2]}{(l_1^2-m^2)(l_2^2-m^2)((l_1+q)^2-m^2)((l_2+q)^2-m^2)}, \tag{B1}$$

where $\delta_+(p^2-m^2)=\theta(p^0)\delta(p^2-m^2)$. One can work out the result of performing integration over l_1^+, l_2^+, l_2^- integrals using the three delta functions. Working out the delta and theta functions for $t=0$ leads to the following:

$$\mathrm{Im}\mathcal{M}^{(2)}_{\mathrm{QCD}} = \frac{g^6}{256\pi^5}\frac{1}{s}\int \mathrm{d}^2\boldsymbol{l}_{1\perp}\mathrm{d}^2\boldsymbol{l}_{2\perp}\frac{\theta(s-(\sqrt{\Delta_1}+\sqrt{\Delta_2}+\sqrt{\Delta_{12}})^2)}{(\Delta_1\Delta_2)^2}I_{l_1^-}, \tag{B2}$$

where

$$I_{l_1^-} = \frac{1}{s}\int_{y_{\min}}^{y_{\max}}\mathrm{d}l_1^-\frac{\sqrt{s}-l_1^-}{l_1^-}\frac{1}{|x_1-x_2|}\sum_{i=1}^{2}(\sqrt{s}+x_i)^2. \tag{B3}$$

In the equation above, the limits of integration are dictated by the theta functions in the cut diagram and $y_{\min}$ and $y_{\max}$ are the smallest and biggest of the roots of the quadratic equation:

$$\sqrt{s}y(\sqrt{s}-y) = \Delta_1 y + (\sqrt{\Delta_2}+\sqrt{\Delta_{12}})^2(\sqrt{s}-y). \tag{B4}$$

In Eq. (B3), x_1, x_2 are the two roots of the quadratic equation (in x):

$$\left(l_1^- - \frac{\Delta_2}{\sqrt{s}+x}\right)\left(x+\frac{\Delta_1}{\sqrt{s}-l_1^-}\right)+\Delta_{12}=0. \tag{B5}$$

Integrand in Eq. (B3) is equal to the fourth order polynomial in the l_1^- divided by a square root of a fourth order polynomial in the denominator and divided by $(l_1^-)^2$. The integrand simplifies if one keeps all the roots of the numerator and denominator (in l_1^-) to the leading order in $s\to\infty$. Then one gets

$$I_{l_1^-} \approx \frac{1}{\sqrt{s}} \int_{\alpha_2}^{\alpha_3} \frac{\mathrm{d}l_1^-}{(l_1^-)^2} \frac{(l_1^- - \beta_1)(l_1^- - \beta_2)(\alpha_3 - l_1^-)}{\sqrt{(l_1^- - \alpha_1)(l_1^- - \alpha_2)}}, \tag{B6}$$

where

$$\alpha_1 = \frac{(\sqrt{\Delta_{12}} - \sqrt{\Delta_2})^2}{\sqrt{s}}, \qquad \alpha_2 = \frac{(\sqrt{\Delta_{12}} + \sqrt{\Delta_2})^2}{\sqrt{s}}, \qquad \alpha_3 = \sqrt{s}, \qquad \beta_{1,2} = \frac{\Delta_{12} \pm \sqrt{\Delta_2}\sqrt{2\Delta_{12} - \Delta_2}}{\sqrt{s}}. \tag{B7}$$

Performing the integral above and keeping the leading $s \to \infty$ term gives

$$I_{l_1^-} \approx \ln \frac{s}{\Delta_{12}} - 2. \tag{B8}$$

The last integral can be done exactly and expanded. It can also be noticed that since the Δ_1 dependence dropped out from all roots in Eq. (B7), and because the original expression was symmetric in Δ_1 and Δ_2 one can could have guessed that the answer is independent on Δ_2 to the leading order as $s \to \infty$. A calculation of the integral in Eq. (B6) with $\Delta_2 = 0$ is much simpler and leads to same result as in Eq. (B8). Thus, we get the final result

$$\mathrm{Im}\mathcal{M}^{(2)}_{\mathrm{QCD}} = \frac{g^6}{256\pi^5} \frac{1}{s} \int d^2\boldsymbol{l}_{1\perp} \mathrm{d}^2\boldsymbol{l}_{2\perp} \frac{\theta(s - (\sqrt{\Delta_1} + \sqrt{\Delta_2} + \sqrt{\Delta_{12}})^2)}{(\Delta_1\Delta_2)^2} \left[\ln \frac{s}{\Delta_{12}} - 2\right]. \tag{B9}$$

Note that this result has been derived assuming that $t = -\boldsymbol{q}_\perp^2 = 0$. Also note that to the leading order in Δ/s the theta function can be set to 1.

2. Modes in the EFT

The two-loop graph in which first momentum is collinear (l_1) and second one is Glauber gluon (l_2) is equal to

$$\mathrm{Im}\mathcal{M}^{(2)}_{nG} = \frac{g^6}{64\pi^5} \int d^4l_1 d^4l_2 \frac{\delta_+[(-l_1^+)(\sqrt{s} - l_1^-) - \Delta_1]\delta_+[(l_1^+ - l_2^+)l_1^- - \Delta_{12}]\delta_+[\sqrt{s}l_2^- - \Delta_2]\theta(\sqrt{s} + l_2^+)}{(l_1^+ l_1^- - \Delta_1)(-\Delta_2)((l_1^+ + q^+)l_1^- - \Delta_{1q})(-\Delta_{2q})}. \tag{B10}$$

The expression above can be found from expanding the full QCD graph in the given momentum region. The integration over l_1^+, l_2^+, l_2^- can be performed using the three delta functions. As a result we get

$$\mathrm{Im}\mathcal{M}^{(2)}_{nG} = \frac{1}{s} \int \mathrm{d}^2\boldsymbol{l}_{1\perp} \mathrm{d}^2\boldsymbol{l}_{2\perp} \frac{\theta(s - (\sqrt{\Delta_{12}} + \sqrt{\Delta_1})^2)}{\Delta_1\Delta_2\Delta_{1q}\Delta_{2q}} I_{l_1^-}, \tag{B11}$$

where

$$I_{l_1^-} = \int_{\Delta_{12}/\sqrt{s}}^{\sqrt{s}} \frac{\mathrm{d}l_1^-}{l_1^-} \frac{\Delta_{1q}}{\Delta_{1q} + (\frac{\Delta_1}{\sqrt{s} - l_1^-} + q^+)l_1^-} = \ln \frac{s}{\Delta_{12}} + \frac{1}{2} \ln \frac{\Delta_{1q}}{\Delta_1} - \frac{\arctan U}{U}. \tag{B12}$$

In the equation above the quantity U equals to

$$U = \sqrt{\frac{4\Delta_1\Delta_{1q}}{(t + \Delta_1 + \Delta_{1q})^2} - 1}. \tag{B13}$$

For all the values of t, Δ_1, Δ_{1q} consistent with their values as a function of $\boldsymbol{l}_{1\perp}, \boldsymbol{l}_{2\perp}, m$ the quantity $U > 0$. Thus, we get the following final result for this two-loop nG loop integral:

$$\mathrm{Im}\mathcal{M}^{(2)}_{nG} = \frac{g^6}{256\pi^5} \frac{1}{s} \int d^2\boldsymbol{l}_{1\perp} \mathrm{d}^2\boldsymbol{l}_{2\perp} \frac{\theta(s - (\sqrt{\Delta_{12}} + \sqrt{\Delta_1})^2)}{\Delta_1\Delta_2\Delta_{1q}\Delta_{2q}} \left[\ln \frac{s}{\Delta_{12}} + \frac{1}{2} \ln \frac{\Delta_{1q}}{\Delta_1} - \frac{\arctan U}{U}\right]. \tag{B14}$$

Similar calculations for the $\mathrm{Im}\mathcal{M}^{(2)}_{G\bar{n}}$ graph leads to an identical result.

APPENDIX C: OVERLAP SUBTRACTION FORMULA

Here, we derive a master formula to account for overlaps given a number of regions. We start by stating certain assumptions about the construction [5]. In the following, a given region is denoted by R_i and the full domain of integration by R. We have

$$R_i \cap \ldots \cap R_j = \emptyset, \qquad R_i \cup \ldots \cup R_j = R. \tag{C1}$$

We also assume that expansions commute; for example, $\mathcal{M}^{(1)}_{n\bar{n}} = \mathcal{M}^{(1)}_{\bar{n}n}$ as easily found in our explicit calculations. The last important property is that an integral converges absolutely within any region if the integrand is expanded appropriately. First, the full integral for N modes is identically equal to

$$\int_R dlI = \sum_{i=1}^{N} \int_{R_i} dlI_i. \tag{C2}$$

With some work, the integral in any given region can be written identically as follows:

$$\begin{aligned}\int_{R_i} dlI_i = {} & \int_R dlI_i - \int_R dl \sum_{j\neq i}^{N} I_{ji} + \int_R dl \sum_{j\neq i}^{N}\sum_{k\neq i}^{N} I_{jki} \\ & - \text{4-fold overlaps} + \cdots \\ & + \int_{R_i} dl \sum_{j\neq i}^{N} I_{ji} - \int_{R_i} dl \sum_{j\neq i}^{N}\sum_{k\neq i}^{N} I_{jki} \\ & + \text{4-fold overlaps} - \cdots.\end{aligned} \tag{C3}$$

Notice that the sums are constrained to avoid double counting under the assumption of commuting expansions. For example, if we have a total of four modes

$$\begin{aligned}\int_{R_1} dlI_1 = {} & \int_R dlI_1 - \int_R dl \sum_{i\neq 1}^{4} I_{i1} + \int_R dl \sum_{i\neq 1}^{4}\sum_{j\neq 1}^{4} I_{ij1} \\ & - \int_R dlI_{3241} + \int_{R_1} dl \sum_{i\neq 1}^{4} I_{i1} - \int_{R_1} dl \sum_{i\neq 1}^{4}\sum_{j\neq 1}^{4} I_{ij1} \\ & + \int_{R_1} dlI_{3241}.\end{aligned} \tag{C4}$$

Now the full result is obtained by adding all the modes to yield

$$\begin{aligned}\int_R dlI = {} & \int_R dl \sum_{i=1}^{N} I_i - \int_R dl \sum_{i=1}^{N}\sum_{j>i}^{N} I_{ij} \\ & + \int_R dl \sum_{i=1}^{N}\sum_{j>i}^{N}\sum_{k>j}^{N} I_{ijk} - \text{four overlaps} + \cdots.\end{aligned} \tag{C5}$$

Note that the order of subscript indices does not matter because expansions commute.

[1] C. W. Bauer, S. Fleming, and M. E. Luke, Phys. Rev. D **63**, 014006 (2000); C. W. Bauer, S. Fleming, D. Pirjol, and I. W. Stewart, Phys. Rev. D **63**, 114020 (2001); M. Beneke, A. P. Chapovsky, M. Diehl, and T. Feldmann, Nucl. Phys. **B643**, 431 (2002).

[2] J. C. Collins and G. F. Sterman, Nucl. Phys. **B185**, 172 (1981); J. C. Collins and D. E. Soper, Annu. Rev. Nucl. Part. Sci. **37**, 383 (1987); J. C. Collins, D. E. Soper, and G. F. Sterman, Adv. Ser. Dir. High Energy Phys.. **5**, 1 (1988).

[3] M. Beneke and V. A. Smirnov, Nucl. Phys. **B522**, 321 (1998).

[4] V. A. Smirnov, Springer Tracts Mod. Phys. **177**, 1 (2002).

[5] B. Jantzen, J. High Energy Phys. 12 (2011) 076.

[6] A. V. Manohar and I. W. Stewart, Phys. Rev. D **76**, 074002 (2007).

[7] J. R. Forshaw and D. A. Ross, Cambridge Lect. Notes Phys. **9**, 1 (1997).

[8] J. C. Polkinghorne, J. Math. Phys. (N.Y.) **4**, 503 (1963); J. Math. Phys. (N.Y.) **4**, 1393 (1963); **4**, 1396 (1963).

[9] R. J. Eden, P. V. Landshoff, D. Olive, and J. C. Polkinghorne, *The Analytic S Matrix* (Cambridge University Press, Cambridge, 1966).

[10] C. W. Bauer, B. O. Lange, and G. Ovanesyan, J. High Energy Phys. 07 (2011) 077.

[11] B. Jantzen, A. V. Smirnov, and V. A. Smirnov, Eur. Phys. J. C **72**, 2139 (2012).

[12] A. Idilbi and A. Majumder, Phys. Rev. D **80**, 054022 (2009); F. D'Eramo, H. Liu, and K. Rajagopal, Phys. Rev. D **84**, 065015 (2011); G. Ovanesyan and I. Vitev, J. High Energy Phys. 06 (2011) 080; Phys. Lett. B **706**, 371 (2012).

[13] J. F. Donoghue and D. Wyler, Phys. Rev. D **81**, 114023 (2010).

[14] S. Fleming, arXiv:1404.5672.

[15] I. I. Balitsky and L. N. Lipatov, Yad. Fiz. **28**, 1597 (1978) [Sov. J. Nucl. Phys. **28**, 822 (1978)]; E. A. Kuraev, L. N. Lipatov, and V. S. Fadin, Zh. Eksp. Teor. Fiz. **72**, 377 (1977) [Sov. Phys. JETP **45**, 199 (1977)].

[16] L. N. Lipatov, Yad. Fiz. **23**, 642 (1976) [Sov. J. Nucl. Phys. **23**, 338 (1976)]; L. L. Frankfurt and V. E. Sherman, Sov. J. Nucl. Phys. **23**, 581 (1976); L. Tyburski, Phys. Rev. D **13**, 1107 (1976); E. A. Kuraev, L. N. Lipatov, and V. S. Fadin, Zh. Eksp. Teor. Fiz. **71**, 840 (1976) [Sov. Phys. JETP **44**, 443 (1976)]; L. N. Lipatov, Zh. Eksp. Teor. Fiz. **90**, 1536 (1986) [Sov. Phys. JETP **63**, 904 (1986)]; V. S. Fadin and L. N. Lipatov, Phys. Lett. B **429**, 127 (1998); A. B. Kaidalov, in *At the Frontier of Particle Physics*, Vol. 1, edited by M. Shifman (World Scientific, Singapore, 2001), pp. 603–636.

[17] J. C. Collins, D. E. Soper, and G. F. Sterman, Nucl. Phys. **B223**, 381 (1983); G. T. Bodwin, Phys. Rev. D **31**, 2616 (1985); **34**, 3932 (1986); J. C. Collins, D. E. Soper, and G. F. Sterman, Nucl. Phys. **B261**, 104 (1985).

[18] J.-Y. Chiu, A. Jain, D. Neill, and I. Z. Rothstein, Phys. Rev. Lett. **108**, 151601 (2012); J. High Energy Phys. 05 (2012) 084.

[19] I. Z. Rothstein and I. W. Stewart (to be published); I. W. Stewart, "Glauber Gluons in SCET" in SCET2010, Ringberg, Germany, https://indico.mpp.mpg.de/conferenceDisplay.py?confId=632; I. Z. Rothstein, "Progress in EFT" in Quantum Fields Beyond Perturbation Theory KITP, Santa Barbara, http://online.kitp.ucsb.edu/online/qft-c14/.